Journal of Solid State Chemistry **152,** 361–373 (2000)
doi:10.1006/jssc.2000.8664, available online at http://www.idealibrary.com on IDEAL®

Structural Chemistry and Electronic Properties of the Hexagonal Perovskites $BaIr_{1-x}Co_xO_{3-\delta}$ ($x = 0.5, 0.7, 0.8$)

Jaap F. Vente* and Peter D. Battle†,[1]

*Departamento de Física Aplicadá, Cinvestav-IPN Unidad Mérida, Carretera Ant. a Progreso km 6, Apartado Postal # 73 Cordemex, 97310, Mérida, Yucatan, México; and †Inorganic Chemistry Laboratory, University of Oxford, South Parks Road, Oxford, OX1 3QR, United Kingdom

Received December 2, 1999; accepted February 24, 2000

The room temperature crystal structures of three compositions in the system $BaIr_{1-x}Co_xO_{3-\delta}$ ($x = 0.5, 0.7, 0.8$) have been determined from X-ray and neutron powder diffraction data. $BaIr_{0.5}Co_{0.5}O_{3.02(1)}$, $BaIr_{0.3}Co_{0.7}O_{2.84(1)}$, and $BaIr_{0.2}Co_{0.8}O_{2.83(1)}$ adopt 12R, 10H, and 5H perovskite structures, respectively; the distribution of Co and Ir cations over corner-sharing and face-sharing sites has been determined, and the Co/Ir–O bond lengths have been used to assign the cation oxidation states as Ir^{5+} and Co^{3+}/Co^{4+}. Arguments based on bond lengths and magnetic susceptibility data have been used to assign spin states; at room temperature $BaIr_{0.5}Co_{0.5}O_{3-\delta}$ contains both high-spin and low-spin Co^{3+}. The distribution of anion vacancies has been determined for $x = 0.7, 0.8$; in the latter case there is evidence for the replacement of some BaO_3 layers in the pseudo-hcp structure by BaO_2 layers, thus introducing tetrahedral transition metal sites which are found to be occupied by Co. Neutron diffraction experiments carried out at 5 K revealed a monoclinic distortion in the $x = 0.5$ sample, with the environment of the high-spin Co^{3+} cation undergoing a Jahn–Teller distortion. The structures of the $x = 0.7$, 0.8 phases did not change significantly on cooling. Measurements of magnetization as a function of applied field suggest that spin glass or cluster glass behavior is present in $x = 0.5, 0.7$ below 50 K. In the case of $x = 0.8$, magnetization and neutron diffraction data suggest the formation of a weak ferromagnet with a saturation magnetization of 0.60 μ_B per Co cation at 5 K.

Key Words: **perovskite; iridium; cobalt.**

INTRODUCTION

The electronic properties of mixed metal oxides have been the focus of much research in the past decade, and materials which adopt perovskite-related structures have been central to this work. The reasons for this include the ability of the perovskite structure to accommodate a wide range of cations on both the 12-coordinate A site and the 6-coordinate B site while retaining the stoichiometry ABO_3. This flexibility in turn derives from the existence of a number of structurally related polymorphs. All perovskites can be considered to consist of stacks of pseudo-close-packed layers, each of stoichiometry AO_3, with the B cations occupying interlayer holes which are octahedrally coordinated by six oxide ions. The wide range of observed structures arises because the layers can be stacked in an hcp sequence, a ccp sequence, or any periodic mixed sequence; the possible sequences are well documented (1). If the local stacking around a particular layer is hcp, then the octahedra on either side of it will have a common face, and if the local stacking around a layer is ccp, the octahedra on either side will share a single vertex. The ability to provide face-sharing and corner-sharing octahedra in different ratios is one of the key features of the perovskite family, with the nature of the B cations determining which polymorph is adopted under ambient conditions; size and electron configuration are among the properties which determine the most stable structure. However, for a given composition the relative stabilities of different polymorphs are also sensitive to temperature and pressure, and phase transitions have been observed in many systems (2). In some cases, usually determined by the redox properties of the B site cation, the oxygen content also changes as a function of temperature and pressure. In view of the sensitivity of the structural chemistry to cation size, redox chemistry, and electron configuration, it is not surprising that changes to the elemental distribution on the B sites are accompanied by structural change. This has been clearly demonstrated in the system $SrMn_{1-x}Fe_xO_{3-\delta}$ (3–5); variations in the concentration ratio of the two transition metals on the 6-coordinate sites produce structural changes and concomitant changes in the electronic properties of the material. A marked change in properties has also been observed in the solid solution $Ba_3CoIr_{2-x}Ru_xO_9$, $0 \le x \le 2$ (6, 7). Although the system adopts the structure of the 6H polymorph (in the notation of (1)) for all values of x, the magnetic behavior changes progressively from that of a weak ferromagnet ($x = 0$) to that of

[1] To whom correspondence should be addressed.

0022-4596/00 $35.00

an antiferromagnet ($x = 2$). The observation of a spontaneous magnetization ($T_c = 108$ K) in $Ba_3CoIr_2O_9$ was particularly interesting in view of the ferromagnetism of metallic $BaIrO_{3-\delta}$ (8), and led us to investigate other mixed Co/Ir perovskites (6, 9). In this paper we describe the structural and magnetic properties of three different perovskite polymorphs in the system $BaIr_{1-x}Co_xO_{3-\delta}$. These phases were first reported (10) by Schaller *et al.*, who identified 12R $BaIr_{0.5}Co_{0.5}O_3$, 10H $BaIr_{0.3}Co_{0.7}O_{3-\delta}$, and 5H $BaIr_{0.2}Co_{0.8}O_{3-\delta}$ by X-ray powder diffraction. However, they did not carry out a full structural characterization, nor did they investigate the magnetic properties of the new phases. The idealized structures of these compounds are drawn in Fig. 1, along with those of 9R $BaIrO_{3-\delta}$ and 2H $BaCoO_3$; the electronic structure of the latter is also of contemporary interest (11). It can be seen that the ratio of face-sharing and vertex-sharing octahedra changes markedly as a function of composition in the $BaIr_{1-x}Co_xO_{3-\delta}$ series, but that all the phases described below retain the trimers which are present in ferromagnetic $BaIrO_{3-\delta}$. Our study of these phases has involved a determination of oxygen content by TGA, a structure determination at room temperature and 5 K by neutron diffraction, and an investigation of their magnetic properties by SQUID magnetometry. We describe the structural chemistry of each phase, paying particular attention to the distribution of vacancies on the oxide sublattice. We also discuss the oxidation states of the Co and Ir cations, and the spin states of the former, in an attempt to rationalize our magnetic data.

EXPERIMENTAL

Black polycrystalline samples of $BaIr_{1-x}Co_xO_{3-\delta}$ were prepared by heating well-ground, pelleted, stoichiometric mixtures of $BaCO_3$, Ir metal, and Co_3O_4 in air at various temperatures between 850 and 1000°C for a total of 1 week. Thereafter the compositions $x = 0.7$ and $x = 0.8$ were heated at 1100°C for 1 week and subsequently air-quenched. The sample $x = 0.5$ was given a different treatment because the intended product was known to be a low-temperature phase. The sample was heated to 1050°C and then slowly cooled (0.05°C min^{-1}) to 850°C, at which temperature it was annealed for 1 week before being air-quenched to room temperature. This procedure was repeated twice to achieve a monophasic product. X-ray powder diffraction data were collected in the angular range $10 \leq 2\theta \leq 120^\circ$ in steps of 0.02° 2θ using a Siemens D5000 diffractometer operating with Cu$K\alpha_1$ radiation in Bragg–Bretano geometry. Neutron diffraction data were collected in the angular range $10 \leq 2\theta \leq 147^\circ$ in steps of 0.05° 2θ, $\lambda = 1.5937$ Å, on the diffractometer D2b at the Institut Laue-Langevin in Grenoble, France. Data were collected both at room temperature and at 5 K for all three compositions studied. The samples ($\sim$5 g) were contained in a 5-mm-diameter vanadium can. The neutron diffraction data were corrected for absorption (12) because of the high absorption cross section of iridium (13). All the diffraction patterns were analyzed by Rietveld refinement (14) using the GSAS suite of programs (15). The room temperature X-ray and neutron data for each composition were analyzed simultaneously. The background levels of all the diffraction patterns were fitted using a shifted Chebyshev polynomial and the peak shapes were described using a pseudo-Voigt function. The oxygen stoichiometry was determined by monitoring the sample mass during the reduction of about 30 mg in a gentle flow of 10% H_2/N_2 while the temperature was raised from 30 to 900°C. Magnetic measurements were performed using a Quantum Design SQUID magnetometer. The susceptibilities were measured in fields of 100 and 1000 G after cooling in both zero field (ZFC) and the measuring field (FC). Hysteresis measurements were carried out at 5 and 300 K between $\pm$ 2 kG after cooling of the sample in a field of 2 kG. Conductivity measurements were performed between 70 and 300 K on sintered bars using a dc four-terminal method. Electrical contacts to the bar were made with silver paint.

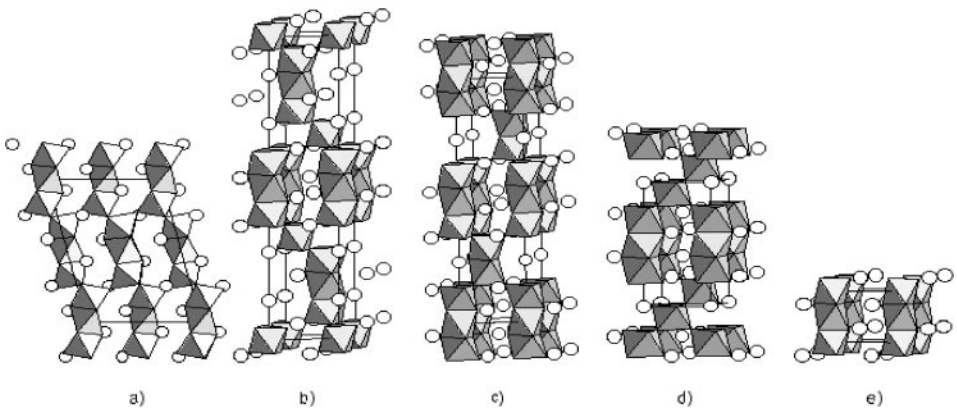

FIG. 1. Crystal structures of (a) 9R $BaIrO_3$, (b) 12R $BaIr_{0.5}Co_{0.5}O_3$, (c) 10H $BaIr_{0.3}Co_{0.7}O_3$, (d) 5H $BaIr_{0.2}Co_{0.8}O_3$, and (e) 2H $BaCoO_3$.

RESULTS

The preparation of the compounds $BaIr_{1-x}Co_xO_{3-\delta}$ proceeded smoothly and the resulting X-ray diffraction patterns were in good agreement with those expected on the basis of the results presented by Schaller *et al.* (10). The TGA data lead to the compositions $BaIr_{0.5}Co_{0.5}O_{3.02(1)}$, $BaIr_{0.3}Co_{0.7}O_{2.87(1)}$, and $BaIr_{0.2}Co_{0.8}O_{2.84(1)}$. In all cases, these values for the oxygen content are slightly higher than those reported previously.

The refinement of the room temperature structure of 12R $BaCo_{0.5}Ir_{0.5}O_{3.02}$, using both X-ray and neutron data, was carried out in space group $R\bar{3}m$ starting from the model provided by Schaller *et al.* (10) The essential features of the cation distribution were established in preliminary refinements in which all the transition metal sites were constrained to be fully occupied, with the same isotropic temperature factor, but with no constraint on the overall composition. Encouragingly, the refined composition was consistent with the Co : Ir ratio used in the chemical synthesis. In light of the results of these preliminary refinements the Co : Ir ratio was constrained to be 1 : 1, with the Co/Ir(3) octahedra that share corners with the trimers occupied only by Co (Fig. 1). Subsequent refinements showed that 89.2% of the central (Co/Ir(1)) octahedra of the trimeric $(Co/Ir)_3O_{12}$ groups are also occupied by Co and that the two outer octahedra (Co/Ir(2)) are occupied almost exclusively (94.6%) by Ir. Refinements of the anion occupation numbers did not reveal a significant concentration of oxygen vacancies in this sample, in agreement with the TGA results. The usual parameters were varied during our structural refinement, but we also included two additional parameters to allow for the anisotropic peak broadening which was apparent in our diffraction data. It is often necessary to use these parameters when modeling this type of structure (16) because the linear dimensions of the crystallites are greater in the xy plane than along the z axis. During the course of the refinements it became apparent that some of the peaks in the difference curve were due to the presence of a low concentration (1% by weight) of the high-temperature 4H modification of $BaCo_{0.5}Ir_{0.5}O_3$. A two-phase refinement technique was subsequently used to take account of the scattering by the impurity, although, with the exception of the concentration, the parameters of the minority phase were held constant after the initial cycles. The two phases were assumed to have the same peak width. The structural parameters of 12R $BaCo_{0.5}Ir_{0.5}O_3$ resulting from this data analysis are listed in Table 1, and the relevant bond lengths and angles are listed in Table 2. The observed and calculated diffraction profiles are shown in Fig. 2. The neutron diffraction data collected at 5 K could not be interpreted within the crystallographic model that had been used successfully in the refinement of the room temperature structure. Additional Bragg reflections were observed, and the fact that some of them occured at $2\theta > 100^\circ$ indicated that the difference was due to a change in the crystal structure rather than to the onset of long-range magnetic ordering. We were able to account for all the peaks in the diffraction pattern using space group $C2/m$, a subgroup of $R\bar{3}m$, and the refinement of the low-temperature structure proceeded smoothly in this monoclinic group, although we were unable to refine the anisotropic thermal factors of the oxide ions. The cation distribution was constrained to that determined at room temperature, as was the concentration of the impurity phase. The structural parameters resulting from this analysis are listed in Table 3, and the relevant bond lengths and angles are listed in Table 4. The observed and calculated diffraction profiles are shown in Fig. 3. The counting statistics are reduced as a consequence of the structural distortion, and the bond lengths determined at 5 K are therefore not as precise as those measured at room temperature. The negative temperature factor of Co/Ir(3) indicates that our structural model (or absorption correction) is imperfect in some way. However, the precision of the

TABLE 1
Structural Parameters of $BaIr_{0.5}Co_{0.5}O_3$ at Room Temperature[a]

Atom	Site	Co fraction	x	y	z	U_{iso}, U_{eq} (Å^2)	U_{11} (Å^2)	U_{22} (Å^2)	U_{33} (Å^2)	U_{12} (Å^2)	$U_{13} = -U_{23}$ (Å^2)
Ba(1)	6*c*		0	0	0.2884(1)	0.010(1)					
Ba(2)	6*c*		0	0	0.1286(1)	0.015(1)					
Co/Ir(1)	3*b*	0.892(8)	0	0	1/2	0.014(2)					
Co/Ir(2)	6*c*	0.054(4)	0	0	0.41040(7)	0.009(1)					
Co/Ir(3)	3*a*	1	0	0	0	0.005(2)					
O(1)	18*h*		0.1515(2)	0.8485(2)	0.45682(6)	0.008	0.010(1)	0.010(1)	0.011(1)	0.006(1)	0.003(1)
O(2)	18*h*		0.1674(2)	0.8326(2)	0.62594(7)	0.008	0.007(1)	0.007(1)	0.013(2)	0.004(1)	−0.001(1)

[a] Space group, $R\bar{3}m$; $a = b = 5.72059(8)$ Å, $c = 28.4073(5)$ Å, $V = 805.09(2)$ Å^3; 1.0(1)% by weight as impurity phase modeled as 4H $BaIr_{0.5}Co_{0.5}O_3$. Agreement indices: neutron, $R_{wp} = 6.64\%$, $R_p = 5.09\%$, DWd = 0.69; X ray, $R_{wp} = 10.08\%$, $R_p = 7.94\%$, DWd = 1.38; totals $R_{wp} = 7.83\%$, $R_p = 7.01\%$, DWd = 1.03, $\chi^2_{red} = 2.05$ for 55 variables.

TABLE 2
Bond Lengths (Å) and Bond Angles (°) for $BaIr_{0.5}Co_{0.5}O_3$ at Room Temperature

Ba(1)–O(1)	2.869(3)	3×	Co/Ir(1)–O(1)	1.939(2)	6×
Ba(1)–O(2)	2.943(3)	3×	Co/Ir(2)–O(1)	1.998(2)	3×
Ba(1)–O(2)	2.8628(2)	6×	Co/Ir(2)–O(2)	1.953(2)	3×
Ba(2)–O(1)	2.8680(2)	6×	Co/Ir(3)–O(2)	2.011(2)	6×
Ba(2)–O(1)	2.927(3)	3×			
Ba(2)–O(2)	2.990(3)	3×	O(1)–O(1)	2.600(3)	
			O(2)–O(2)	2.848(4)	
O(1)–Co/Ir(1)–O(1)	84.24(8)		O(1)–Co/Ir(2)–O(1)	81.20(9)	
			O(1)–Co/Ir(2)–O(2)	170.6(1)	
O(2)–Co/Ir(3)–O(2)	90.20(9)		O(2)–Co/Ir(2)–O(2)	94.6(1)	

refined parameters is consistent with the discussion that follows.

The refinement of the structure of 10H $BaIr_{0.3}Co_{0.7}O_{2.87}$ using X-ray and neutron diffraction data proceeded without major difficulties using the starting model provided by Schaller *et al.* (10) in space group $P6_3/mmc$. An approach similar to that described above was used. The cation ordering between cobalt and iridium proved to be rather different from that found in 12R $BaCo_{0.5}Ir_{0.5}O_3$, with Ir preferentially occupying the central octahedra (Co/Ir(1)) of the trimers, rather than the outer sites (Co/Ir(2)). The cation sites within the M_2O_9 dimers (Co/Ir(3)) were constrained to have the same Co/Ir content as the outer octahedra of the trimers, with which they share corners. Releasing the compositional constraints did not change the partial occupancies significantly. Preliminary refinements in which the anisotropic thermal parameters of the oxide ions were refined together with their fractional occupancies indicated that the anion vacancies revealed by our TGA experiments are confined to the O(3) site, which is located at the center of the M_2O_9 dimers, wherein the cobalt ions are concentrated. The structural parameters resulting from our data analysis are listed in Table 5, and the relevant bond lengths and angles are listed in Table 6. The observed and calculated diffraction profiles are shown in Fig. 4. The neutron diffraction data collected at 5 K could be interpreted using the same crystallographic model and no additional reflections which could be of magnetic origin were observed. The anisotropic thermal parameters (Table 7) U_{11} and U_{22} of O(3) show no decrease between room temperature and 5 K, in contrast with U_{33} and the corresponding parameters of O(1) and O(2). This is consistent with the presence of static disorder in the xy plane on the O(3) sublattice. We note that the change in length (Table 8) of the Co/Ir(3)–O(3) bond length on cooling is greater than that of any other bond listed in Table 6.

The analysis of the room temperature X-ray and neutron diffraction data collected from the compound 5H $BaIr_{0.2}Co_{0.8}O_{2.83}$ proved to be more complicated. The cobalt–iridium distribution is again partially disordered. The central position of the triple group (Co/Ir(1)) was found to be occupied by both Co and Ir in almost equal amounts, while the outer position (Co/Ir(2)) is mainly occupied by Co (75.6(5)%). The two polyhedra (Co/Ir(3)) that link the trimers, and are linked together by corner sharing in the ideal structure, are occupied exclusively by Co. Once this was established, largely from the information contained in the X-ray diffraction pattern, we attempted to characterize the oxide sublattice, relying heavily on the neutron diffraction data. The $(Co/Ir)_3O_{12}$ trimers in the ideal 5H structure of this compound are separated by two corner-sharing octahedra. During the early stages of the analysis, the oxide ion at the shared vertex showed anomalous thermal parameters, indicatative of significant disorder in the xy plane at $z \sim 0$, and it became clear that the observed diffraction data

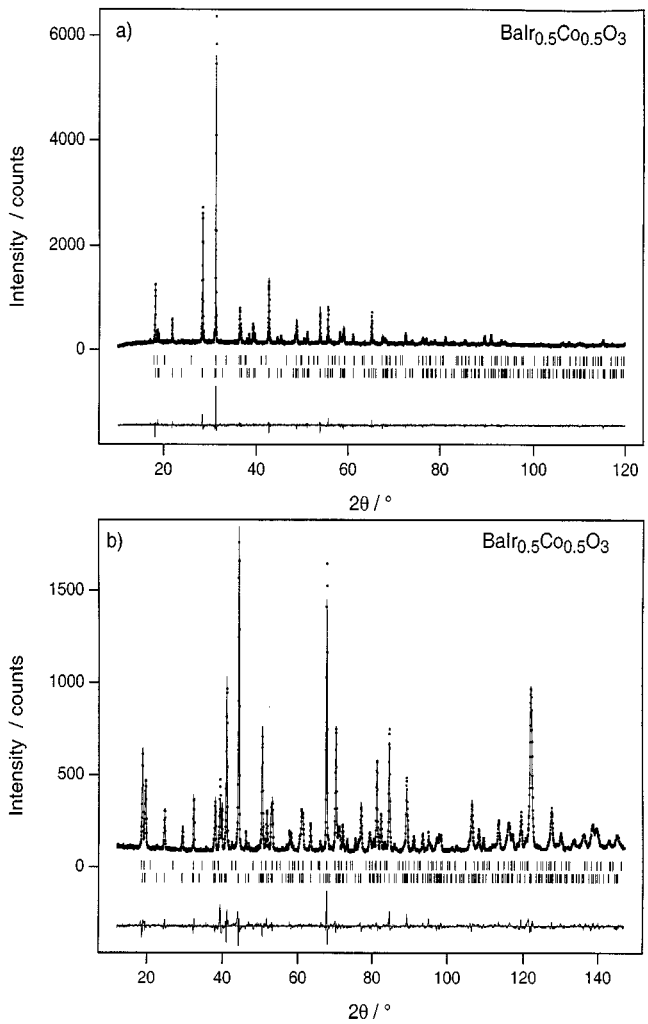

FIG. 2. Observed, calculated, and difference (a) X-ray and (b) neutron diffraction patterns of 12R $BaIr_{0.5}Co_{0.5}O_3$ at room temperature. Reflection positions are marked for both the minority (upper) and majority (lower) phases.

TABLE 3
Structural Parameters of $BaIr_{0.5}Co_{0.5}O_3$ at 5 K[a]

Atom	Site	Co fraction	x	y	z	U_{iso} (Å^2)
Ba(1)	4*i*		0.7147(9)	0	0.1347(6)	0.000(1)
Ba(2)	4*i*		0.8767(9)	0	0.6155(7)	0.008(1)
Co/Ir(1)	2*d*	0.892	1/2	0	1/2	0.003(3)
Co/Ir(2)	4*i*	0.054	0.4055(5)	0	0.2307(3)	0.003(1)
Co/Ir(3)	2*a*	1	0	0	0	−0.013(3)
O(1)	8*j*		0.1211(5)	0.7284(8)	0.6270(5)	0.004(1)
O(2)	8*j*		−0.0484(6)	0.750(1)	0.1228(6)	0.003(1)
O(3)	4*i*		0.3927(7)	0	0.6317(8)	0.002(2)
O(4)	4*i*		0.1987(8)	0	0.119(1)	0.009(1)

[a] Space group, $C2/m$; $a = 9.8359(4)$, $b = 5.7299(3)$ Å, $c = 10.0421(4)$ Å, $\beta = 109.786(3)^\circ$, $V = 532.55(3)$ Å^3; 1.0% by weight as impurity phase modeled as 4H $BaIr_{0.5}Co_{0.5}O_3$. Agreement indices (neutron): $R_{wp} = 7.30\%$, $R_p = 5.65\%$, DWd = 0.59, $\chi^2_{red} = 3.75$ for 49 variables.

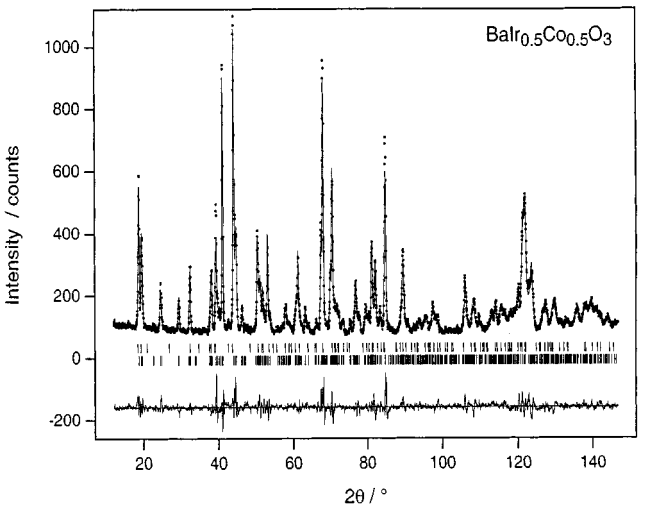

FIG. 3. Observed, calculated, and difference neutron diffraction patterns of 12R $BaIr_{0.5}Co_{0.5}O_3$ at 5 K. Reflection positions are marked for both the minority (upper) and majority (lower) phases.

were not consistent with the idealized structure. Further refinements were carried out in which the BaO_3 layer between the two octahedra was replaced by a BaO_2 layer of the type observed in 12H $BaCoO_{2.6}$ (17). The reduction of this layer results in the replacement of the two corner-sharing octahedra by two unconnected tetrahedra. Neither of the two models gave an entirely satisfactory fit, although it became clear that the model in which Co/Ir(3) is coordinated by four oxide ions is more compatible with the diffraction data than that in which it is in six-fold coordination. We therefore devised a combination of the two models, such that Co/Ir(3) was coordinated by either four or six oxide ions. In order to achieve this we used two sites, O(1) and O(2), with the sum of their fractional occupancies constrained to unity. The difference in the site multiplicities of O(1) and O(2) allows variation in the total oxygen content within this model; $0 \le \delta \le 0.2$ in the formula $BaIr_{0.2}Co_{0.8}O_{3-\delta}$. A simultaneous refinement of X-ray and neutron data based on the disordered model produced a greatly improved fit, with a total oxygen content that was in agreement with our TGA measurements (albeit with rather large values for the thermal parameters of O(1) and O(2)). The refinement quality improved further once the presence of an impurity phase was recognized. This impurity phase, 1.5(2)% by weight, was modeled as 10H $BaCo_{0.7}Ir_{0.3}O_3$. The final structural parameters resulting from these refinements are listed in Table 9 and the corresponding bond lengths and angles are listed in Table 10. The diffraction profiles are shown in Fig. 5. A refinement (Fig. 6) performed using the data collected at 5 K resulted in a very similar structure, but three weak peaks, not observed at room temperature, remained unexplained. They could be indexed as 0 0 3/2 at a d-spacing of 7.97 Å; 1 0 1/2 and 0 0 5/2 at 4.80 Å; 1 0 3/2 at 4.19 Å. As no unidentified peaks were observed at lower d-spacings, we concluded that these new peaks were magnetic in origin. The presence of half-integral l values is an indication that the c lattice parameter of the magnetic cell is double that of the nuclear cell, and that the magnetic structure therefore contains an antiferromagnetic component. The presence of 00l reflections indicates that the magnetic moments are not aligned along z. Several models were tested, but we were unable to find a magnetic structure that was consistent with both the neutron data and the magnetization data discussed below. The sparcity of magnetic Bragg intensity prevented the testing of complex, non-collinear magnetic models. The

TABLE 4
Bond Lengths (Å) and Bond Angles (°) for $BaIr_{0.5}Co_{0.5}O_3$ at 5 K

Ba(1)–O(1)	2.852(8)	2×	Ba(2)–O(1)	2.833(9)	2×
Ba(1)–O(2)	2.77(1)	2×	Ba(2)–O(1)	2.897(7)	2×
Ba(1)–O(2)	2.925(8)	2×	Ba(2)–O(1)	2.833(9)	2×
Ba(1)–O(2)	2.93(1)	2×	Ba(2)–O(2)	2.966(8)	2×
Ba(1)–O(3)	2.88(1)	1×	Ba(2)–O(3)	2.8708(7)	2×
Ba(1)–O(4)	2.95(1)	1×	Ba(2)–O(3)	2.96(1)	1×
Ba(1)–O(4)	2.8707(7)	2×	Ba(2)–O(4)	2.99(1)	1×
Co/Ir(1)–O(1)	1.932(5)	4×	Co/Ir(2)–O(1)	2.019(5)	2×
Co/Ir(1)–O(3)	1.951(8)	2×	Co/Ir(2)–O(2)	1.940(6)	2×
Co/Ir(3)–O(2)	2.049(5)	4×	Co/Ir(2)–O(3)	1.997(8)	1×
Co/Ir(3)–O(4)	1.915(8)	2×	Co/Ir(2)–O(4)	1.963(9)	
O(1)–O(3)	2.593(7)				
O(1)–Co/Ir(1)–O(1)	85.3(2)		O(1)–Co/Ir(2)–O(1)	80.9(3)	
O(1)–Co/Ir(1)–O(3)	84.6(2)		O(1)–Co/Ir(2)–O(2)	170.0(3)	
O(2)–Co/Ir(3)–O(2)	91.3(4)		O(1)–Co/Ir(2)–O(3)	81.2(2)	
O(2)–Co/Ir(3)–O(4)	91.2(2)		O(1)–Co/Ir(2)–O(4)	92.7(4)	
			O(3)–Co/Ir(2)–O(4)	172.0 (5)	

TABLE 5
Structural Parameters of $BaIr_{0.3}Co_{0.7}O_{2.84}$ at Room Temperature[a]

Atom	Site	Occupancy (Co or O)	x	y	z	U_{iso}, U_{eq} (Å^2)	U_{11} (Å^2)	U_{22} (Å^2)	U_{33} (Å^2)	U_{12} (Å^2)	$U_{13} = -U_{23}$ (Å^2)
Ba(1)	2*b*		0	0	1/4	0.011(1)					
Ba(2)	4*f*		1/3	2/3	0.1430(1)	0.014(1)					
Ba(3)	4*f*		1/3	2/3	0.5453(1)	0.010(1)					
Co/Ir(1)	2*a*	0.296(8)	0	0	0	0.010(1)					
Co/Ir(2)	4*e*	0.801(2)	0	0	0.1072(1)	0.010(1)					
Co/Ir(3)	4*f*	0.801(2)	1/3	2/3	0.6928(2)	0.014(1)					
O(1)	12*k*		0.1530(2)	0.8470(2)	0.0523(1)	0.008	0.010(1)	0.010(1)	0.010(1)	0.006(1)	0.000(1)
O(2)	12*k*		0.8342(2)	0.1658(2)	0.1515(1)	0.015	0.013(1)	0.013(1)	0.027(2)	0.008(1)	0.001(1)
O(3)	6*h*	0.714(8)	0.5198(5)	0.0397(9)	1/4	0.024	0.012(2)	0.055(4)	0.030(3)	0.029(2)	0

[a]Space group, $P6_3/mmc$, $a = b = 5.70747(8)$ Å, $c = 23.8462(4)$ Å, $V = 672.70(2)$ Å^3. Agreement indices: neutron, $R_{wp} = 5.17\%$, $R_p = 4.00\%$, DWd = 0.90; X ray, $R_{wp} = 7.87\%$, $R_p = 6.18\%$, DWd = 1.54; totals, $R_{wp} = 6.21\%$, $R_p = 5.55\%$, DWd = 1.24, $\chi^2_{red} = 1.65$ for 58 variables.

values obtained for the refined structural parameters at 5 K are listed in Table 11.

The temperature dependence of the molar magnetic susceptibility of $BaIr_{0.5}Co_{0.5}O_3$ measured in 100 G is shown in Fig. 7a. The inset shows the inverse susceptibility in the high-temperature region. The corresponding data for $BaIr_{0.3}Co_{0.7}O_{2.84}$ and $BaIr_{0.2}Co_{0.8}O_{2.83}$ are given in Figs. 7b and 7c, respectively. The data collected in a field of 1000 G were qualitatively very similar to those shown. The susceptibility data for the three compounds look similar. The insets show that the ZFC and FC data overlie in the high-temperature region and that they can be described adequately by a Curie–Weiss expression modified to include a correction for temperature-independent paramagnetism (T.I.P.). The parameters derived from this model are listed in Table 12. All three compounds have a positive Weiss temperature (θ), indicating the dominance of ferromagnetic interactions. At temperatures below T_c a marked but limited increase in the FC susceptibility of the three compounds is observed, whereas the ZFC susceptibility passes through a maximum. The low magnitude of this increase is inconsistent with a transition to a ferromagnetic state, but could indicate the formation of either a cluster glass or a weakly ferromagnetic (canted antiferromagnet) state. The temperature of the magnetic transition decreases with increasing Co content, whereas the Weiss temperature increases. To resolve the nature of this transition we measured the magnetization at 300 and 5 K as a function of applied field after cooling in the maximum field. The central parts of these curves are depicted in Fig. 8. All the curves recorded at 300 K have a negligible width, are linear, and pass through the origin, showing that the samples are in a paramagnetic state. However, at 5 K, the $M(H)$ curves of $BaIr_{0.5}Co_{0.5}O_3$ and $BaIr_{0.3}Co_{0.7}O_{2.84}$ have a finite width and are not symmetrical around the origin. This is consistent with a spin glass or cluster glass state but not with a WFM state. The $M(H)$ behavior of $BaIr_{0.2}Co_{0.8}O_{2.83}$ at 5 K is very different, with clear hysteresis in a magnetization curve which is symmetrical around the origin and reaches, in fields as low as $\sim$200 G, a saturation value of 2660(3) emu mole^{-1}, corresponding to 0.60 μ_B per Co or, assuming that Co(1) is diamagnetic, 0.66 μ_B per magnetic Co. Taken together, the magnetization data and the neutron data described above show that the 5H phase is a weak ferromagnet below 18 K.

The temperature dependence of the electrical resistivity of the three compounds studied is presented in Fig. 9. All show thermally activated behavior but the absolute values of the conductivity are relatively (18) high for mixed metal oxides of Ir. The activation energies are of the order of 50 meV (Table 12) and slightly temperature dependent.

TABLE 6
Bond Lengths (Å) and Bond Angles (°) for $BaIr_{0.3}Co_{0.7}O_{2.84}$ at Room Temperature

Ba(1)–O(2)	2.865(2)	6×	Co/Ir(1)–O(1)	1.961(2)	6×
Ba(1)–O(3)	2.8603(3)	6×	Co/Ir(2)–O(1)	2.001(3)	3×
Ba(2)–O(1)	2.803(3)	3×	Co/Ir(2)–O(2)	1.949(3)	3×
Ba(2)–O(2)	2.8606(3)	6×	Co/Ir(3)–O(2)	1.927(3)	3×
Ba(2)–O(3)	3.148(4)	3×	Co/Ir(3)–O(3)	1.992(4)	3×
Ba(3)–O(1)	2.8616(2)	6×	O(1)–O(1)	2.620(3)	
Ba(3)–O(1)	2.932(3)	3×	O(2)–O(2)	2.839(4)	
Ba(3)–O(2)	3.024(3)	3×	O(3)–O(3)	2.513(8)	
O(1)–Co/Ir(1)–O(1)	83.8(1)				
O(1)–Co/Ir(2)–O(1)	81.8(1)		O(2)–Co/Ir(3)–O(2)	96.2(2)	
O(1)–Co/Ir(2)–O(2)	171.9(2)		O(2)–Co/Ir(3)–O(2)	167.5(2)	
O(2)–Co/Ir(2)–O(2)	93.5(2)		O(3)–Co/Ir(3)–O(3)	78.2(2)	

DISCUSSION

The transition metal cations in the 12R phase $BaIr_{0.5}Co_{0.5}O_3$ have a mean oxidation state of +4.

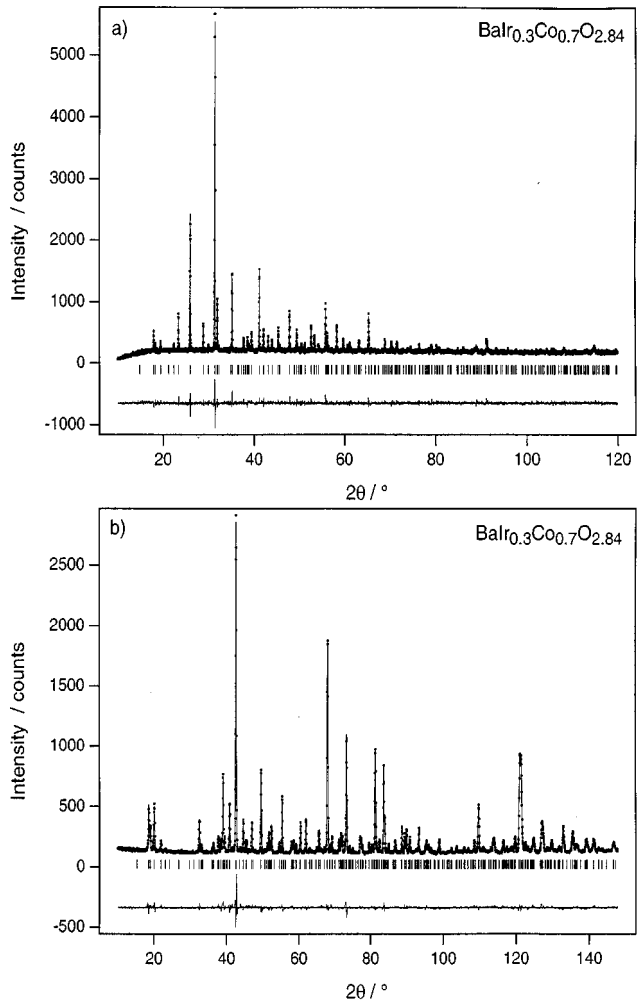

FIG. 4. Observed, calculated, and difference (a) X-ray and (b) neutron diffraction patterns of 10H $BaIr_{0.3}Co_{0.7}O_{2.84}$ at room temperature. Reflection positions are marked.

$BaLaCoIrO_6$ has previously been shown to contain Co^{2+} and low-spin Ir^{5+} (6, 9), and it therefore seems reasonable to expect the true oxidation states in $BaIr_{0.5}Co_{0.5}O_3$ to be Co^{3+} and Ir^{5+}. The bond lengths listed in Table 1 can be interpreted in a way which lends support to this hypothesis. Ignoring the relatively low level of cation disorder, the mean bond length (1.976 Å) around the Ir(2) site is close to that (1.98 Å) observed in $BaLaCoIrO_6$ and somewhat shorter than that (2.047 Å) measured in the Ir^{4+} oxide Sr_4IrO_6. The Co(1)–O bond length (1.939 Å) is comparable to that (1.92 Å) at the low-spin, 6-coordinate Co^{3+} site in Co_3O_4, but in order to account for the Co–O distance (2.011 Å) around the Co(3) site we must assume that the Co^{3+} cation is, unusually, in a high-spin state. We are thus proposing that the environments of these two sites are sufficiently different to stabilize two different spin states of Co^{3+} in this compound. In view of the nonmagnetic ground state of Ir^{5+} (19), the Co(3) cations are the only paramagnetic species in this phase and the molar Curie constant (0.75, Table 12) of $BaIr_{0.5}Co_{0.5}O_3$ is consistent with this conclusion, being in excellent agreement with the value calculated for 0.25 moles of $S = 2$ cations. It is difficult to discuss the cation ordering scheme adopted in $BaIr_{0.5}Co_{0.5}O_3$ because very few comparable sytems have been studied previously. The M_2O_9 dimers are occupied by Ir^{5+} in 6H $Ba_3CoIr_2O_9$ (6), but the Co in that compound is divalent rather than trivalent, and it is dangerous to discuss the behavior of transition metals without taking account of all the relevant factors; low-spin Co^{3+} is certainly closer in size to Ir^{5+} than is Co^{2+}, and the trivalent cation is also more likely to be found in a low-spin state. The structural distortion which occurs between room temperature and 5 K produces one striking change in the coordination geometry of the transition metal cations. At room temperature, Co/Ir(3) is located in a nearly regular octahedron with M–O distances of 2.011(2) Å and O–Co–O bond angles of 90.20(9)°. However, at 5 K this

TABLE 7
Structural Parameters of $BaIr_{0.3}Co_{0.7}O_{2.84}$ at 5 K[a]

Atom	Site	Occupancy (Co or O)	x	y	z	U_{iso}, U_{eq} (Å^2)	U_{11} (Å^2)	U_{22} (Å^2)	U_{33} (Å^2)	U_{12} (Å^2)	$U_{13} = -U_{23}$ (Å^2)
Ba(1)	2*b*		0	0	1/4	0.004(1)					
Ba(2)	4*f*		1/3	2/3	0.1431(2)	0.007(1)					
Ba(3)	4*f*		1/3	2/3	0.5456(2)	0.009(1)					
Co/Ir(1)	2*a*	0.296	0	0	0	0.007(1)					
Co/Ir(2)	4*e*	0.801	0	0	0.1069(2)	0.009(1)					
Co/Ir(3)	4*f*	0.801	1/3	2/3	0.6933(2)	0.007(1)					
O(1)	12*k*		0.1531(2)	0.8469(2)	0.0525(1)	0.005	0.005(1)	0.005(1)	0.006(1)	0.004(1)	−0.001(1)
O(2)	12*k*		0.8349(3)	0.1651(3)	0.1516(1)	0.010	0.008(1)	0.008(1)	0.017(1)	0.004(1)	0.000(1)
O(3)	6*h*	0.714	0.5210(5)	0.042(1)	1/4	0.020	0.012(2)	0.060(3)	0.020(3)	0.030(2)	0

[a]Space group, $P6_3/mmc$; $a = b = 5.69217(9)$ Å, $c = 23.7865(4)$ Å, $V = 66745(2)$ Å^3. Agreement indices (neutron): $R_{wp} = 5.32\%$, $R_p = 4.15\%$, DWd = 0.90, $\chi^2_{red} = 2.36$ for 45 variables.

[b]Fixed at room temperature values.

TABLE 8
Bond Lengths (Å) and Bond Angles (°) for $BaIr_{0.3}Co_{0.7}O_{2.84}$ at 5 K

Ba(1)–O(2)	2.852(2)	6×	Co/Ir(1)–O(1)	1.959(2)	6×
Ba(1)–O(3)	2.8538(4)	6×	Co/Ir(2)–O(1)	1.989(3)	3×
Ba(2)–O(1)	2.793(4)	3×	Co/Ir(2)–O(2)	1.943(4)	3×
Ba(2)–O(2)	2.8533(4)	6×	Co/Ir(3)–O(2)	1.933(4)	3×
Ba(2)–O(3)	3.146(5)	3×	Co/Ir(3)–O(3)	1.969(5)	3×
Ba(3)–O(1)	2.8540(3)	6×			
Ba(3)–O(1)	2.933(4)	3×	O(3)–O(3)	2.48(1)	
Ba(3)–O(2)	3.017(4)	3×			
O(1)–Co/Ir(1)–O(1)	83.7(1)				
O(1)–Co/Ir(2)–O(1)	82.2(2)		O(2)–Co/Ir(3)–O(2)	96.0(2)	
O(1)–Co/Ir(2)–O(2)	172.5(2)		O(2)–Co/Ir(3)–O(2)	167.6(3)	
O(2)–Co/Ir(2)–O(2)	93.0(2)		O(3)–Co/Ir(3)–O(3)	78.2(3)	

octahedron shows a strong Jahn–Teller distortion with four long (Co–O = 2.049(5) Å) and two short bond lengths (Co–O = 1.915(8) Å); the mean bond length thus remains essentially unchanged at 2.004 Å. This distortion stabilizes the t_{2g} orbital which contains the lone β spin electron, and thus effectively quenches any orbital contribution to the magnetic moment of the Co^{3+} cation. The excellent agreement with the spin-only magnetic moment over a wide temperature range suggests that local distortions may be present at relatively high temperatures, and that they drive a cooperative phase transition on cooling. The shape of the distorted octahedron (four long bonds, two short) is unusual. It is also inconsistent with the use of a model involving an intermediate spin state ($t_{2g}^5\, e_g^1$) for the Co^{3+} cations (20), which would lead to the stabilization of four short bonds and two long bonds, as is usual in Jahn–Teller systems. The environments of the Ir and Ba cations distort less markedly in response to the symmetry lowering, and the mean bond lengths change very little.

If we assume that the transition metal oxidation states in 10H $BaIr_{0.3}Co_{0.7}O_{3-\delta}$ are also Ir^{5+} and Co^{3+}, we arrive at a composition $BaIr_{0.3}Co_{0.7}O_{2.80}$, i.e., $\delta = 0.2$, a value somewhat greater than that determined experimentally by both neutron diffraction ($\delta = 0.17$) and TGA ($\delta = 0.13$). Assuming that the Ir remains pentavalent, averaging the two results leads to a mean oxidation state of $Co^{+3.14}$ (86% Co^{3+}, 14% Co^{4+}) in this phase, a significantly higher value than was observed in the 12R material. A previous study of 12H $BaCoO_{2.6}$ (17) showed that Co^{4+} has a preference for tetrahedral sites, and we have therefore interpreted the data on 10H $BaIr_{0.3}Co_{0.7}O_{2.85}$ in terms of a model which locates the oxidized Co cations on the site Co/Ir(3), with the partially vacant site O(3) within the coordination shell. Assuming a random distribution of vacancies over the O(3) sublattice, 18% of the cation sites within the Co/Ir(3) dimers will be 4-coordinated by oxygen. If we assume that the larger Ir cations do not occupy 4-coordinate sites, then 0.07 Co cations per formula unit are 4 coordinate. This is less than the total number (0.10) of Co^{4+} cations per formula unit, and some Co^{4+} cations must therefore occupy sites with a higher coordination number. As in the case of the 12H phase, a distorted tetrahedral geometry will favor (21) a high spin state, $S = 5/2$ for Co^{4+}. The Co/Ir(1)–O distance agrees well with the concentration-weighted mean of appropriate low-spin Co^{3+}–O and Ir^{5+}–O distances (22), but the mean Co/Ir(2)–O and Co/Ir(3)–O distances are longer than expected for low-spin Co^{3+}, and imply that these sites contain paramagnetic Co, even though there are no vacancies in the coordination sphere. We return to this point below. The O(1)–O(1) distances (defining the shared octahedral face within the trimers) are short enough to

TABLE 9
Structural parameters of $BaIr_{0.2}Co_{0.8}O_{2.83}$ at Room Temperature[a]

Atom	Site	Occupancy (Co or O)	x	y	z	U_{iso}, U_{eq} (Å²)	$U_{11} = U_{22}$ (Å²)	U_{33} (Å²)	U_{12} (Å²)	$U_{13} = -U_{23}$ (Å²)
Ba(1)	1*a*		0	0	0	0.016(1)				
Ba(2)	2*d*		1/3	2/3	0.7777(3)	0.008(1)				
Ba(3)	2*d*		1/3	2/3	0.4129(3)	0.014(1)				
Co/Ir(1)	1*b*	0.49 (1)	0	0	1/2	0.006(1)				
Co/Ir(2)	2*c*	0.754 (5)	0	0	0.2885(3)	0.004(1)				
Co/Ir(3)	2*d*	1	1/3	2/3	0.1327(7)	0.014(2)				
O(1)	2*d*	0.85(1)[b]	1/3	2/3	−0.0072(5)	0.048	0.085(3)	0.016(3)	0.041(2)	0
O(2)	3*e*	0.15(1)[b]	1/2	1/2	0	0.08(1)				
O(3)	6*i*		0.1626(2)	0.8374(2)	0.1955(2)	0.008	0.005(1)	0.017(1)	0.003(1)	0.001(1)
O(4)	6*i*		0.1514(2)	0.8486(2)	0.6031(3)	0.006	0.003(1)	0.013(1)	0.000(1)	−0.002(1)

[a] Space group, $P\bar{3}m$; $a = b = 5.7179(1)$ Å, $c = 11.9865(2)$ Å, $V = 339.39(1)$ Å^3; 1.5(2)% by weight as impurity phase modeled as 10H $BaIr_{0.3}Co_{0.7}O_3$. Agreement indices: neutron, $R_{wp} = 4.63\%$, $R_p = 3.64\%$, DWd = 1.05; X ray, $R_{wp} = 6.95\%$, $R_p = 5.53\%$, DWd = 1.82; totals, $R_{wp} = 5.53\%$, $R_p = 4.90\%$, DWd = 1.47, $\chi^2 = 1.39$ for 64 variables.

[b] Constraint: Frac(O(1)) + Frac(O(2)) = 1.

TABLE 10
Bond Lengths (Å) and Bond Angles (°) for $BaIr_{0.2}Co_{0.8}O_{2.83}$ at Room Temperature

Ba(1)–O(1)	3.3024(2)	6×	85%	Co/Ir(1)–O(4)	1.943(2)	6×	
Ba(2)–O(2)	2.85895(4)	6×	15%	Co/Ir(2)–O(3)	1.958(3)	3×	
Ba(1)–O(3)	2.844(2)	6×		Co/Ir(2)–O(4)	1.984(3)	3×	
Ba(2)–O(1)	2.577(7)	1×	85%	Co/Ir(3)–O(1)	1.677(8)	1×	85%
Ba(2)–O(2)	3.133(3)	3×	15%	Co/Ir(3)–O(2)	2.293(4)	3×	15%
Ba(2)–O(3)	2.8770(5)	6×		Co/Ir(3)–O(3)	1.851(4)	3×	
Ba(2)–O(4)	2.762(4)	3×		O(3)–O(3)	2.789(4)		
Ba(3)–O(3)	3.106(4)	6×		O(4)–O(4)	2.597(3)		
Ba(3)–O(4)	2.8694(3)	6×					
O(4)–Co/Ir(1)–O(4)	83.9(2)			O(1)–Co/Ir(3)–O(3)	114.0(2)		
O(3)–Co/Ir(2)–O(3)	90.8(2)			O(2)–Co/Ir(3)–O(2)	77.15(8)		
O(3)–Co/Ir(2)–O(4)	173.7(2)			O(2)–Co/Ir(3)–O(3)	87.3(1)		
O(4)–Co/Ir(2)–O(4)	81.8(2)			O(3)–Co/Ir(3)–O(3)	104.6(3)		

Comment: O(1)–O(2) = 1.6528(3) Å, but these positions are never occupied simultaneously.

provide some shielding of the cation–cation interactions, but they are not as short as the distances found in the shared face within the dimers (O(3)–O(3)).

Whereas the oxide vacancies in 10H $BaIr_{0.3}Co_{0.7}O_{2.84}$ are randomly distributed over the sites on the common face of two octahedra in a $(Co/Ir)_2O_9$ dimer, those in 5H $BaCo_{0.2}Co_{0.8}O_{2.83}$ occur in a more ordered fashion at the common vertices of octahedra which are not linked to any other $(Co/Ir)O_6$ groups by face sharing; such sites do not exist in the $BaIr_{0.3}Co_{0.7}O_{2.84}$ structure, but anion vacancies are known to be located there in other hexagonal perovskites (4). The data in Table 9 can be taken to mean that 85% of the layers having the ideal stoichiometry $Ba(1)O(2)_3$ actually have the stoichiometry $Ba(1)O(1)_2$, although the reduced layers do not occur in a periodic manner along *z*. The mean cation oxidation state in this phase is 3.66, and we shall again assume that all Ir is pentavalent. This implies a mean Co oxidation state of +3.325, that is 32.5% Co^{4+},

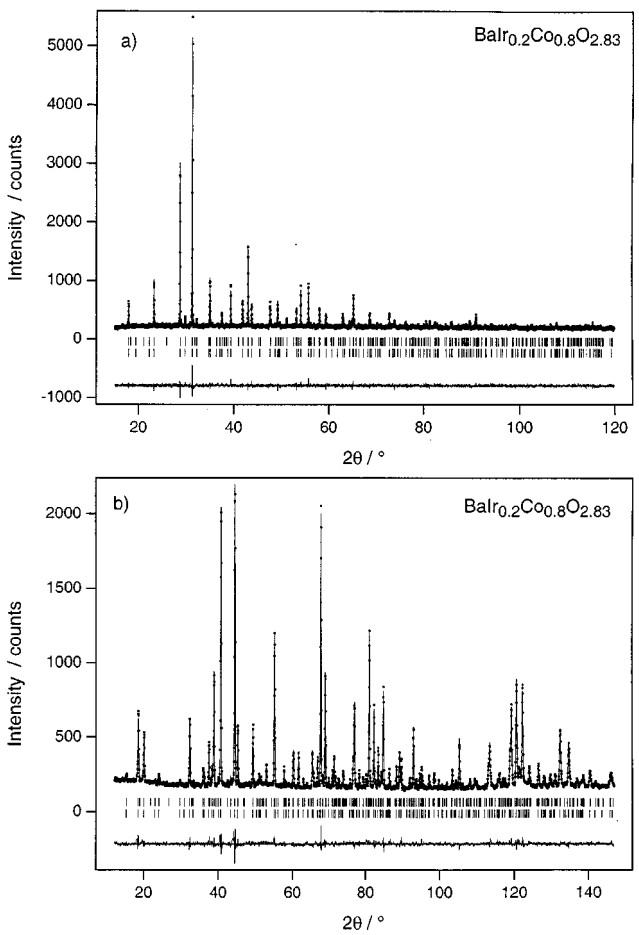

FIG. 5. Observed, calculated, and difference (a) X-ray and (b) neutron diffraction patterns of 5H $BaIr_{0.2}Co_{0.8}O_{2.83}$ at room temperature. Reflection positions are marked for both the minority (upper) and majority (lower) phases.

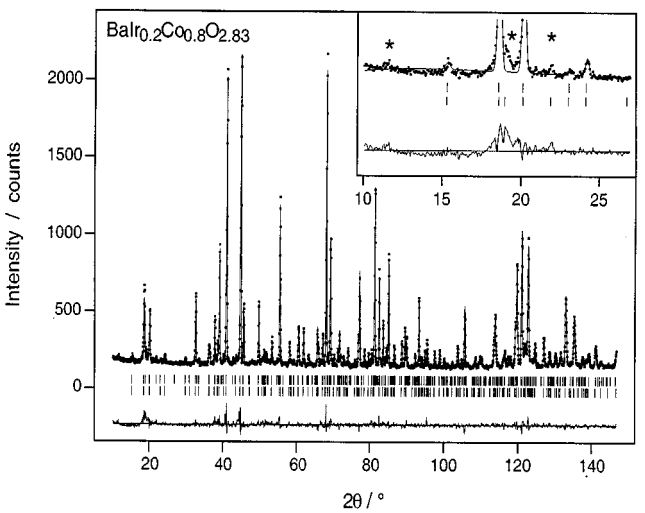

FIG. 6. Observed, calculated, and difference neutron diffraction patterns of 5H $BaIr_{0.2}Co_{0.8}O_{2.83}$ at 5 K. Reflection positions are marked for the minority (upper) and the majority (lower) phases. Magnetic Bragg peaks are marked (*) in the inset.

TABLE 11
Structural Parameters of $BaIr_{0.2}Co_{0.8}O_{2.83}$ at 5 K[a]

Atom	Site	Occupancy (Co or O)	x	y	z	U_{iso}, U_{eq} (Å^2)	$U_{11} = U_{22}$ (Å^2)	U_{33} (Å^2)	U_{12} (Å^2)	$U_{13} = -U_{23}$ (Å^2)
Ba(1)	1*a*		0	0	0	0.011(1)				
Ba(2)	2*d*		1/3	2/3	0.7788(4)	0.005(1)				
Ba(3)	2*d*		1/3	2/3	0.4132(4)	0.008(1)				
Co/Ir(1)	1*b*	0.49	0	0	1/2	0.001(1)				
Co/Ir(2)	2*c*	0.754	0	0	0.2892(3)	0.003(1)				
Co/Ir(3)	2*d*	1	1/3	2/3	0.1326(6)	0.006(2)				
O(1)	2*d*	0.85	1/3	2/3	−0.0070(5)	0.041	0.072(3)	0.018(3)	0.036(2)	0
O(2)	3*e*	0.15	1/2	1/2	0	0.06(2)				
O(3)	6*i*		0.1623(2)	0.8377(2)	0.1955(3)	0.003	−0.001(1)	0.012(1)	0.000(1)	0.001(1)
O(4)	6*i*		0.1517(2)	0.8483(2)	0.6034(3)	0.003	0.000(1)	0.009(1)	−0.001(1)	−0.001(1)

[a] Space group, $P\bar{3}m$, $a = b = 5.70442(7)$ Å, $c = 11.9608(2)$ Å, $V = 337.06(1)$ Å^3; 1.5(2)% by weight as impurity phase modeled as 10H $BaIr_{0.3}Co_{0.7}O_3$. Agreement indices (neutron): $R_{wp} = 5.28\%$, $R_p = 3.98\%$, DWd = 0.711, $\chi^2 = 2.99$ for 44 variables.
[b] Fixed at room temperature values.

67.5% Co^{3+}, or a formula of $BaIr_{0.2}Co^{4+}_{0.26}Co^{3+}_{0.54}O_{2.83}$. The fractional occupancy of the O(1) site (Table 9) leads to a value of 0.34 tetrahedral Co ion per formula unit, which we assume to be 0.26 Co^{4+} and 0.08 Co^{3+}, all in a high spin state. The tetrahedral Co(3) site modeled in our refinements is irregular, but the mean Co–O bond length is comparable

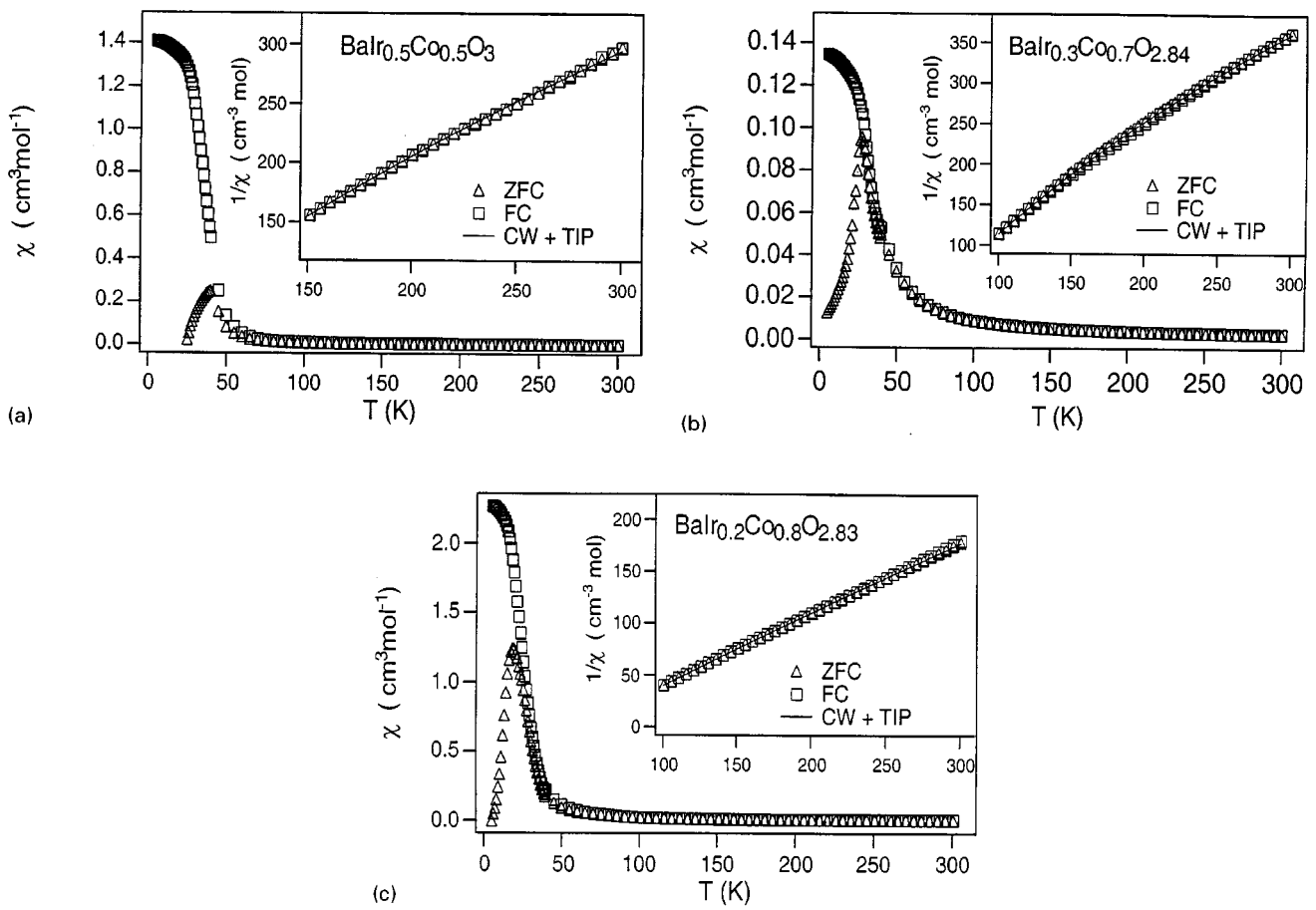

FIG. 7. Temperature dependence of FC and ZFC susceptibility of (a) 12R $BaIr_{0.5}Co_{0.5}O_3$, (b) 10H $BaIr_{0.3}Co_{0.7}O_{2.84}$, and (c) 5H $BaIr_{0.2}Co_{0.8}O_{2.83}$. The insets show fits to the high-temperature data using a Curie–Weiss law with an additional temperature-independent term.

to those in other Co^{4+} compounds (23, 24). Assuming that all the remaining, 6-coordinate Co^{3+} is in a low spin state, this model leads to a molar Curie constant of 1.38 emu, in excellent agreement with the value determined experimentally. However, this level of agreement may be fortuitous because the 15% of the Co(3) sites which are 6-coordinate, although smaller than the corner-sharing sites in 12R $BaIr_{0.5}Co_{0.5}O_3$, are certainly large enough to accommodate high-spin Co^{3+}. Furthermore, the Co/Ir(2) site at the end of the trimers is also large enough to accommodate high-spin Co^{3+} along with 24.6% Ir^{5+}. The bond lengths around Co/Ir(1) are consistent with this site, which

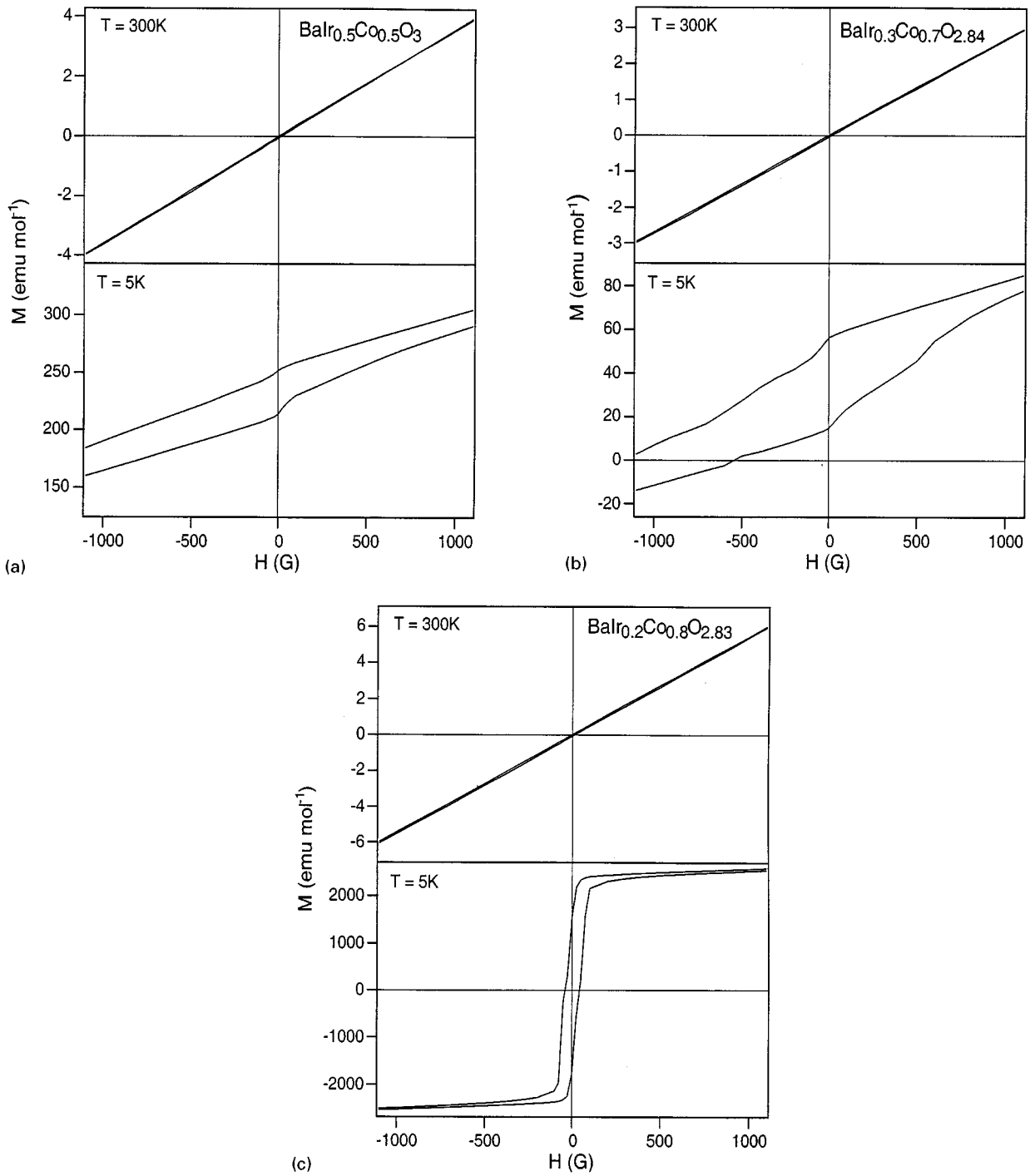

FIG. 8. Magnetization as a function of applied field at 300 and 5 K for (a) 12R $BaIr_{0.5}Co_{0.5}O_3$, (b) 10H $BaIr_{0.3}Co_{0.7}O_{2.84}$, and (c) 5H $BaIr_{0.2}Co_{0.8}O_{2.83}$.

TABLE 12
Electronic Properties of $BaIr_{1-x}Co_xO_{3-\delta}$

x	0.5	0.7	0.8
Structure	12R	10H	5H
ρ_{290K} (Ω cm)	0.06	0.25	3.0
E_a (meV) 220–290 K	63	54	140
120–175 K	54	69	88
T_c (K)	38	31	18
C ($cm^3\,mol^{-1}\,K^{-1}$)	0.75(2)	0.522(7)	1.364(5)
θ (K)	20 (2)	35.0(8)	45.4(2)
T.I.P (10^{-4} $cm^3\,mol^{-1}$)	7.1(4)	8.0(3)	2.8(3)

is only involved in face sharing, being occupied by low-spin Co^{3+} and Ir^{5+}. Despite the transition from short-range to long-range magnetic ordering, there is no significant change in the crystal structure of the 5H phase on cooling to 5 K.

The availability of the relatively straightforward 12R phase $BaIr_{0.5}Co_{0.5}O_3$ as a point of reference allows us to have some confidence in our assignment of cation oxidation states in the more complex 10H and 5H phases. However, the arguments used above in assigning spin states to the cations on the octahedral sites are undoubtedly weaker, and we must therefore be cautious in our interpretation of the magnetic data collected on these phases at low temperatures. The positive Weiss constant derived for 12R $BaIr_{0.5}Co_{0.5}O_3$ from the data in Fig. 7a suggests that ferromagnetic interactions dominate in this phase. The FC magnetization does increase markedly below 38 K, diverging from the FC data, but the displaced FC hysteresis loop observed at 5 K, together with the absence of magnetic Bragg scattering in the low-temperature neutron diffraction pattern, demonstrates that this composition behaves as a spin glass or cluster glass and does not show long-range magnetic ordering. We conclude that the magnetic interactions within this phase are frustrated by a combination of competing interactions, topology, and cation disorder. The high-temperature magnetism of the 10H phase is not as easy to interpret as that of the 12R composition. The observed Curie constant is too small to be consistent with the concentration of paramagnetic cations proposed above on the basis of bond length data; that model results in only 0.085 diamagnetic Co cation per formula unit. The most likely explanations are that the spin state assignments based on the bond lengths are wrong, or that extensive antiferromagnetic coupling takes place between cations in the vacancy-free dimers, thus reducing the number of cations which contribute to the paramagnetism. The latter explanation is not unreasonable in view of the magnetic behavior of other hexagonal perovskites (2, 16, 25). Although we have ruled out the presence of an intermediate spin (IS) state in the 12R phase, the presence of spin-paired dimers along with IS Co^{3+} on the Co/Ir(2) site would largely account for both the bond lengths and the Curie constant of the $x = 0.7$ material. 10H $BaIr_{0.3}Co_{0.7}O_{3-\delta}$ has a glass transition temperature of 31 K. Again, the formation of a magnetic glass is likely to be caused by the frustration created by the presence of competing ferromagnetic and antiferromagnetic interactions; the strength of the former is indicated by the positive value of θ. In the case of the 10H phase, the magnetic superexchange pathways will also be disrupted by the structural disorder around the Co/Ir(3) site. The formation of well-defined BaO_2 layers in 5H $BaIr_{0.2}Co_{0.8}O_{2.83}$ apparently reduces the level of structural disorder to a point where long-range magnetic ordering can occur. The appearance of new Bragg reflections suggests an antiferromagnetic structure, but the magnetization data, which are symmetrical about the origin (Fig. 8c) demonstrate the presence of a soft ferromagnetic component. We therefore conclude that the 5H phase is a weak ferromagnet (a canted antiferromagnet). However, the same uncertainties in spin state assignment are present in this composition as in the 10H phase; the calculated Curie constant can be reduced to the measured value only by invoking antiferromagnetic coupling of neighboring polyhedra or by assuming that either low-spin cations occupy unusually large octahedra, or that an intermediate spin state is present.

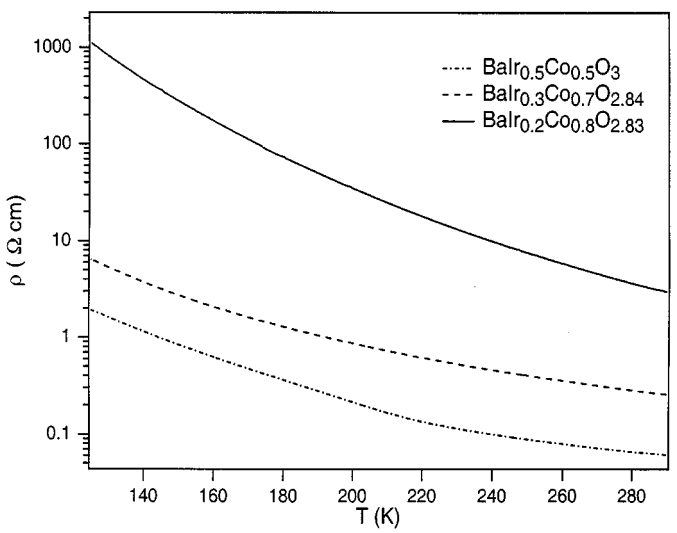

FIG. 9. Electrical resistivity as a function of temperature for 12R $BaIr_{0.5}Co_{0.5}O_3$, 10H $BaIr_{0.3}Co_{0.7}O_{2.84}$, and 5H $BaIr_{0.2}Co_{0.8}O_{2.83}$.

To summarize, the structural chemistry of the perovskite system $BaIr_{1-x}Co_xO_{3-\delta}$ is strongly dependent on the ratio of the two Group 9 transition metals, as are the concentration and distribution of anion vacancies. Significant ferromagnetic coupling is present in all the compositions studied, but long-range magnetic order is established only in the 5H phase. A striking structural distortion occurs on cooling the 12R phase, which contains both high-spin and low-spin Co^{3+}. Our data are not consistent with the

presence of Co^{3+} in an intermediate spin state in the 12R phase, but this may be the cause of the reduced Curie constant in the 10H phase.

ACKNOWLEDGMENTS

We are grateful to the UK EPSRC for the provision of financial support, including neutron diffraction facilities at ILL Grenoble, and to Thomas Hansen for assisting with the data collection.

REFERENCES

1. A. L. Patterson and J. S. Kasper, *in* "International Tables for X-ray Crystallography," Vol. II. Kynoch, Birmingham, 1959.
2. B. L. Chamberland, A. W. Sleight, and J. F. Weiher, *J. Solid State Chem.* **1,** 506 (1970).
3. P. D. Battle, T. C. Gibb, and C. W. Jones, *J. Solid State Chem.* **74,** 60 (1988).
4. P. D. Battle, C. M. Davison, T. C. Gibb, and J. F. Vente, *J. Mater. Chem.* **6,** 1187 (1996).
5. E. J. Cussen, J. Sloan, J. F. Vente, P. D. Battle, and T. C. Gibb, *Inorg. Chem.* **37,** 6071 (1998).
6. P. D. Battle, J. G. Gore, R. C. Hollyman, and A. V. Powell, *J. Alloys Compds.* **218,** 110 (1995).
7. P. Lightfoot and P. D. Battle, *J. Solid State Chem.* **89,** 174 (1990).
8. A. V. Powell and P. D. Battle, *J. Alloys Compds.* **191,** 313 (1993).
9. A. V. Powell, J. G. Gore, and P. D. Battle, *J. Alloys Compds.* **201,** 73 (1993).
10. H. U. Schaller, S. Kemmler-Sack, and A. Ehmann, *J. Less-Common Met.* **97,** 299 (1984).
11. C. Felser, K. Yamaura, and R. J. Cava, *J. Solid State Chem.* **146,** 411 (1999).
12. K. Weber, *Acta Crystallogr. C* **23,** 720 (1967).
13. V. F. Sears, *Neutron News* **3,** 26 (1992).
14. H. M. Rietveld, *J. Appl. Crystallogr.* **2,** 65 (1969).
15. A. C. Larson and R. B. von-Dreele, General Structure Analysis System (GSAS), Report LAUR 86-748, Los Alamos National Laboratories, Los Alamos, NM, 1990.
16. E. J. Cussen, J. F. Vente, and P. D. Battle, *J. Am. Chem. Soc.* **121,** 3958 (1999).
17. A. J. Jacobson and J. L. Hutchison, *J. Solid State Chem.* **35,** 334 (1980).
18. J. G. Gore and P. D. Battle, *J. Mater. Chem.* **6,** 201 (1996).
19. K. Hayashi, G. Demazeau, M. Pouchard, and P. Hagenmuller, *Mater. Res. Bull.* **16,** 1013 (1980).
20. J. B. Goodenough, *Mater. Res. Bull.* **6,** 967 (1971).
21. G. A. Candela, A. H. Kahn, and T. Negas, *J. Solid State Chem.* **7,** 360 (1973).
22. G. Thornton, B. C. Tofield, and A. W. Hewat, *J. Solid State Chem.* **61,** 301 (1986).
23. M. Jansen, *Z. Anorg. Allg. Chem.* **417,** 35 (1975).
24. H. Mattausch and H. Müller-Buschbaum, *Z. Anorg. Allg. Chem.* **386,** 1 (1971).
25. A. Callaghan, C. W. Moeller, and R. Ward, *Inorg. Chem.* **5,** 1572 (1966).